



Title	Stable and efficient collection of single photons emitted from a semiconductor quantum dot into a single-mode optical fiber
Author(s)	Kumano, Hidekazu; Harada, Takumi; Suemune, Ikuo; Nakajima, Hideaki; Kuroda, Takashi; Mano, Takaaki; Sakoda, Kazuaki; Odashima, Satoru; Sasakura, Hiroataka
Citation	Applied Physics Express (APEX), 9(3), 032801 https://doi.org/10.7567/APEX.9.032801
Issue Date	2016-03
Doc URL	http://hdl.handle.net/2115/64558
Rights	© 2016 The Japan Society of Applied Physics
Type	article (author version)
File Information	kumano_APEX03.pdf



[Instructions for use](#)

Stable and efficient collection of single photons emitted from a semiconductor quantum dot into a single-mode optical fiber

Hidekazu Kumano*¹, Takumi Harada¹, Ikuo Suemune¹, Hideaki Nakajima¹, Takashi Kuroda², Takaaki Mano², Kazuaki Sakoda², Satoru Odashima³, and Hiroataka Sasakura⁴

¹*Research Institute for Electronic Science (RIES), Hokkaido University, Sapporo 001-0021, Japan*

²*National Institute for Materials Science (NIMS), Tsukuba 305-0044, Japan*

³*Department of Mechanical Engineering, Hachinohe Institute of Technology, Hachinohe 031-8501, Japan*

⁴*Creative Research Institution (CRIS), Hokkaido University, Sapporo 001-0021, Japan*

We study stable and efficient coupling of single photons generated from a quantum dot (QD) into a single-mode fiber (SMF) prepared in a fiber couple module (FCM). We propose a method to focus the objective lens to a sample surface without imaging with the help of laser reflection. By assembling all the constituents, i.e., a pair of lenses, the SMF, and the optical alignment to the QD source, we demonstrate stable single-photon count rate and a high collection efficiency of 43.5 % of the photons emitted in air from the QD into the collection lens in the FCM.

The Internet of Things (IoT)¹⁾ has been rapidly progressing recently, and everything will be involved in the network in near future. In such a society, secure and trustable communication is getting increasingly important, and cryptography works as a fundamental platform to provide a privacy preserving authentication and confidentiality to legitimate users. However the present cryptography relies on the computational difficulty, and we cannot completely eliminate the latent risk of the system being disabled by some emerging technologies. Quantum key distribution (QKD)²⁾ is expected to be a method to cope with such situations, since it can offer absolute security that cannot be breached, even with high-performance computers or algorithms. When information is encoded on single photons, the security is assured quantum mechanically on the condition that ideal single photon sources (SPSs) and detectors can be employed. Implementation of solid-state SPSs is one of the limited choices to realize deterministic SPSs and for future large-scale system integration, with the probability of generating higher number of photons at a time being nearly zero.

From this perspective, semiconductor quantum dots (QDs) have been intensively studied and the SPSs^{3,4)} working in O-band⁵⁾ and C-band⁶⁾ have been demonstrated. However, for a QD embedded in a bulk semiconductor, a large difference of the refractive indices at the semiconductor-air interface tends to prevent photon extraction to the air-side. When the critical angle for total internal reflection is θ_{CR} , the photon extraction efficiency is given by

*E-mail address: kumano@es.hokudai.ac.jp

$\eta_{extract}=(1-\cos\theta_{CR})/2$.⁷⁾ In the case of an InAs QD embedded in GaAs, the difference of the refractive indices is $\Delta n \approx 2.4$ and θ_{CR} is 17.1° . This gives $\eta_{extract} = 0.022$, and 97.8% of photons emitted from an InAs QD are lost via the total internal reflection at the interface.

A variety of attempts at better collection of the emitted photons have been reported.^{8–20)} One important approach is to collect photons by tailoring the divergence angle by introducing dielectric antenna and the solid immersion lens.^{8–10)} Photonic nanowire waveguides,^{11–14)} horn structure,^{15,16)} and micropillars^{17,18)} with metallic microreflectors^{19,20)} drastically improve the external photon collection efficiency. The next important issue is the realization of efficient coupling of these SPSs to single-mode fibers (SMFs). There have been attempts at coupling SPSs laterally to SMFs by employing tapered nanofibers,^{21–23)} and photon coupling efficiencies of 6–7% have been observed.^{21,22)} Since the coupling is based on the evanescent field extended to SPSs attached on the outer face of nanofibers, it is crucially dependent on the nanofiber diameters. Although a higher efficiency of 22% has been reported for a reduced nanofiber diameter of 350 nm,²³⁾ the reduced diameter results in mechanical instability during practical applications. Simpler methods for coupling SPSs to an SMF facet have been proposed. One of these involves the insertion of photon emitters to the space between two SMF connector facets, and bidirectional single-photon emission has been demonstrated using this method.²⁴⁾ Coupling of SPS based on a semiconductor photonic crystal (PhC) cavity to an SMF was also attempted by pasting a semiconductor PhC sheet to an SMF facet,²⁵⁾ but background emission outside the PhC cavity also coupled to the SMF and increased the background photon emission of the SPS. Highly efficient coupling was predicted through simulations by assuming a quantum emitter pasted on a fiber facet of a tapered nanofiber,²⁶⁾ but an experimental demonstration requires rather advanced setups.

In this letter, we demonstrate efficient coupling of single photons emitted from InAs QDs to a fiber couple module (FCM) and demonstrate long-term stability of the fiber coupled SPS. The FCM includes a photon collection lens with high numerical aperture (NA), an SMF, and an additional lens to couple to the SMF. A QD photon source is placed on a piezo positioner to control the relative position of the QD source and the photon collection lens, and the whole system is set in one body. The most critical issue for high-efficiency operation is the optimal adjustment of the focal length, which is difficult for extremely weak single photon emission. We demonstrate that reflection measurements of an exciting laser offer us efficient tools for this purpose. We also note that the focal length deviation between the exciting laser wavelength and the emitted single photon wavelength needs to be taken care of owing to the lens refractive-index dispersion.

As a QD source, 1.6 ML-InAs QDs embedded in a 150-nm-thick InAlAs barrier layer were grown on an InP (111)A substrate^{27,28)} by droplet epitaxy.²⁹⁾ Since droplet epitaxy is not strain-driven, it is beneficial to tailor photon wavelength and quantum confinement

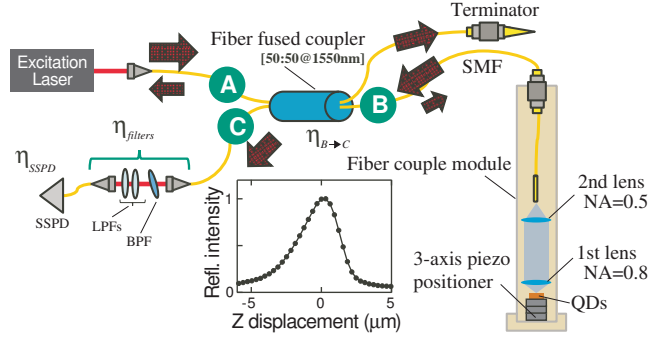


Fig. 1. Schematic of our optical setup to evaluate coupling efficiency between a QD-based single photon source and an SMF. A photon collection lens (NA=0.8), and a second lens (NA=0.5) for coupling to the SMF, and the SMF constitute the fiber couple module (FCM). The QD sample is set on a 3-axis piezo positioner fixed mechanically to the FCM with a SUS304 solid housing. The transmittance efficiency η_{sys} of our setup outside the FCM after the input port B is given by the product of $\eta_{B \rightarrow C} \cdot \eta_{filters} \cdot \eta_{SSPD} = 0.60 \times 0.5 \times 0.15 = 0.045$, where $\eta_{B \rightarrow C}$, $\eta_{filters}$, and η_{SSPD} are the transmittance efficiencies of the 2x2 fiber fused coupler (FFC), the set of filters, and the detection efficiency of the SSPD, respectively. (Inset) Measured laser reflection against the Z-axis displacement (310nm/step @RT) of the QD sample. A laser diode at a wavelength of 940 nm was used, and the positive displacement reduces the distance between the sample surface and the collection lens. The peak position is set to zero displacement, which is used as a reference position for focusing to the sample surface.

by relieving the constraint of material selection. To precisely evaluate the photon coupling efficiency to our FCM, an as-grown planar structure containing the QD sources was employed in this work. A schematic of our optical setup for coupling single photons emitted from QDs to an SMF is shown in Fig. 1. An excitation laser is introduced to port A of a 2x2 fiber fused coupler (FFC), and one output port B is connected to the FCM and the other to a terminator. The laser light reflected from the sample surface or photons emitted from the InAs QDs couple to the FCM and go back to the FFC port B, and transmit to the counterpart ports. The output to the port C is employed for fundamental optical characterization of our setup. The reflected laser is measured with a power meter and the photons emitted from the InAs QDs with a monochromator equipped with a liquid-nitrogen-cooled InGaAs photodiode array. A pair of superconducting single-photon detectors (SSPDs) by Single Quantum BV is also employed for demonstrating the SPS operation. The FCM is composed of an SMF and a pair of aspheric lenses (NA, clear aperture, effective focal length)=(0.8, 1.2 mm ϕ , 0.745 mm) and (0.5, 2 mm ϕ , 2.0 mm) to form an infinity optical system. It collects photons emitted from the QD source and couples photons to the SMF (Thorlabs 980HP, NA=0.2, core=3.6 $\mu\text{m}\phi$). The InAs QD source is fixed on a three-axis piezo positioner that is mechanically fixed to the FCM in a SUS 304 solid housing. The three-axis piezo positioner works over a wide temperature range

covering liquid helium to room temperature (RT).

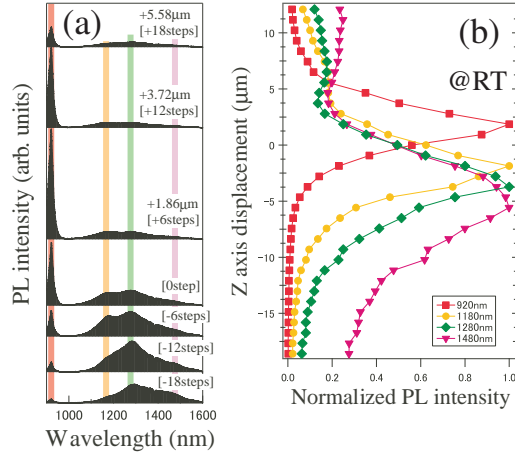


Fig. 2. (a) PL spectra of the InAs dot ensemble measured at RT at several Z-axis positions (310nm/step) around the reference focus position (0 step). (b) PL intensity changes at the four representative wavelengths (hatched area at 920, 1180, 1280, and 1480 nm in (a)) are summarized as a function of Z displacement.

Since the signal intensity from the QDs is too weak to use for adjusting the focus position, 940-nm laser reflection at the sample surface was used to seek the focus position. The inset in Fig. 1 shows the variation of the reflection intensity during the Z-axis scan. Rather sensitive detection of the focus position is possible within the one step scan accuracy of $\sim 0.3 \mu\text{m}$. This enables us to obtain the reference focus position set at the wavelength of 940 nm. It is noted that the Z-axis distance required for obtaining the laser reflection is $\sim 5 \mu\text{m}$ against the effective focal length of 0.745 mm owing to the high NA of the collection lens. We excited the InAs QDs sample at the reference focus position set at the wavelength of 940 nm. We reduced the excitation laser wavelength to 780 nm by employing a Ti:Sapphire laser to study the whole emission spectra from the sample. Even at room temperature, we could observe the photoluminescence (PL) spectra from the QD ensemble, which suggests the high coupling efficiency of our optical setup. Since the QDs have broad size distribution, we observe the broad PL spectrum from 1100 nm to 1600 nm as shown by the “0 step” in Fig. 2(a). An additional PL peak from the InP substrate is observed at around 920 nm. When the sample Z position is changed from the reference focus position, the PL spectra changed sensitively as shown in Fig. 2(a). The dependence of the PL intensity on the Z-axis displacement is plotted in Fig. 2(b) for several specific wavelengths. The positive and negative displacement gives a shorter and longer distance to the FCM, respectively. The intensity peak at the wavelength of 920 nm shifts to the shorter distance from the reference focus position, while it shifts to the longer distance systematically at wavelengths longer than 940 nm. This is attributed to

the refractive-index dispersion of the lenses in the FCM. The shorter (longer) wavelength results in a higher (lower) refractive index and therefore a shorter (longer) focal length. This result shows that we have to pay sufficient attention in the measurements of relatively wide luminescence spectra through optical-fiber measurement setup.

To evaluate the collection efficiency of photons emitted from a single QD quantitatively, we assume that each pulsed laser excitation generates one photon from the QD. Then the efficiency can be simply calculated from the excitation pulse repetition rate and the photon detection rate. For this purpose, we employ the InAs QD sample with the relatively low QD density of $3 \times 10^9 \text{ cm}^{-2}$ and cool down the sample to 4.2 K to maintain almost 100% internal quantum efficiency for the photon emission process. We set the FCM housing including the InAs QDs sample close to the liquid He level in a liquid He vessel. Figure 3(a) shows the PL spectra measured with different continuous-wave (CW) excitation laser powers. Well-resolved single-QD emission lines were observed. The excitation power dependence of the integrated intensity of the peak at a wavelength of 1063 nm (1059 nm) is shown in Fig. 3(b), and it exhibits the linear (bilinear) dependence. From this, we assign the 1063 nm (1059 nm) peak as a neutral exciton X^0 (biexciton XX^0) emission. Figure 3(c) shows the luminescence time decay of the X^0 emission measured with 5-ps pulsed excitation at a wavelength of 760 nm under a repetition rate of 76.08 MHz. The decay time constant derived from the single exponential fit to the measurements is 3.24 ns.

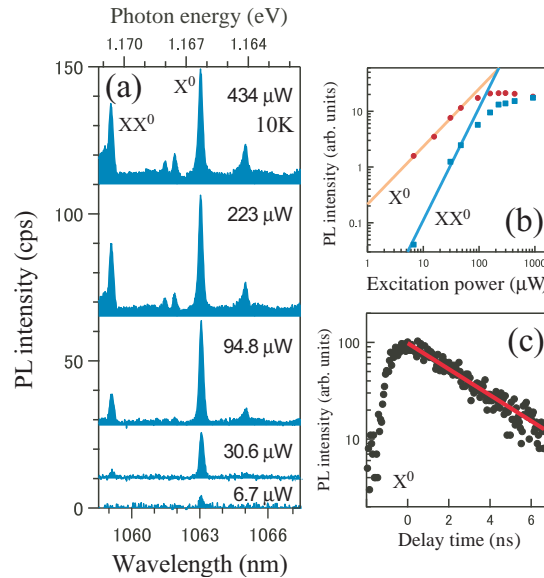


Fig. 3. (a) Excitation power dependence of PL spectra of a single InAs quantum dot measured at 10K. Neutral biexciton (XX^0) and exciton (X^0) lines are observed at 1059 nm and 1063 nm, respectively. (b) Integrated intensities of XX^0 and X^0 as a function of the excitation power. (c) Time-resolved PL measurement of the X^0 line. Decay time constant (τ_e) fitted by the red line is 3.24 ns.

To examine single-photon emission operation of the InAs QD, we work on the second-order photon correlation measurements employing the Hanbury-Brown and Twiss setup under the pulsed excitation power at a QD emission saturation. The measured correlation function is shown in Fig. 4 against the relative delay time τ of the two SSPD outputs. The dip at zero delay exhibits the photon anti-bunching, suggesting single-photon emission from the QD. However, the correlation function profile around the zero delay time appears as the overlap of the reduced peak and dip. The dip profile is generally observed in CW photon correlation measurements.³⁰⁾ The time-resolved measurement shown in Fig. 3(c) exhibits the distinct slow rise after the pulsed excitation around the zero delay time. The photo-excitation at the wavelength of 760 nm generates electrons and holes in the InAlAs barrier. The constituent InAs and AlAs have a large difference in their energy gaps and this induces large potential fluctuations in the InAlAs alloy. The observed slow rise in Fig. 3(c) suggests relatively delayed capture of photo-generated carriers into the InAs QD owing to the slow diffusion through the alloy layer. This will result in the CW-like anti-bunching dip in Fig. 4 superposed on the correlation function generally measured with pulsed operations.

To account for this measured photon correlation function quantitatively, we incorporate the CW-like contribution to the general correlation function.³¹⁾ Considering the present condition of the luminescence decay time constant $\tau_e = 3.24$ ns and the pulse excitation interval $T=13.14$ ns and therefore $\tau_e/T \ll 1$, the generalized photon correlation function is given by

$$N^{-1} \left\{ B + \sum_n \exp \left(-\frac{|\tau - nT|}{\tau_e} \right) \cdot \left\{ 1 - \alpha_0 \exp \left(-\left(G + \frac{1}{\tau_e} \right) |\tau| \right) \right\} \right\}, \quad (1)$$

where B , α_0 , G , and N are the background counts, degree of multiphoton contribution ($0 \leq \alpha_0 \leq 1$), the excitation rate, and normalization factor, respectively. We obtain the fitted result denoted by the solid curve in Fig. 4. Both the dip depth at $\tau = 0$ and the nominal peak height at $\tau \sim 0$ are well reproduced. This fitting leads to $B=0.004$, $G = 0.74$ ns⁻¹, $N \simeq 1$, and the parameter $\alpha_0=0.71$, which gives the value of $g^{(2)}(0)=0.29$.

Under the pulsed excitation of the InAs QD at a repetition rate of 76.08 MHz, the photon count rate measured with the SSPD in the setup of Fig. 1 was 10,400 cps. Therefore the net single photon count rate is estimated to be $10,400\sqrt{1 - g^{(2)}(0)}$ by compensating the multiple photon emission probability³²⁾ and is 8,760 cps. This value can be equated with $1/T \cdot \eta_{QD} \cdot \eta_{extract} \cdot \eta_{collect} \cdot \eta_{FCE} \cdot \eta_{sys}$, where η_{QD} , η_{FCE} , η_{sys} , and $\eta_{collect}$ are the internal quantum efficiency of the QD, the fiber coupling efficiency of the second lens, the system efficiency of our optical setup including the detector's quantum efficiency ($\eta_{SSPD}=0.15$ at $\lambda=1060$ nm according to manufacturer's specification sheet), and the photon collection efficiency to the first lens, respectively. We assume $\eta_{QD} = 1$ at saturation and at low temperature. We worked on separate measurements of η_{FCE} and η_{sys} and obtained values of 0.267 and 0.045,

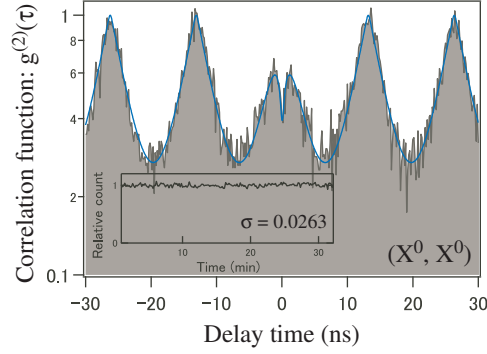


Fig. 4. Second-order photon correlation function for the X^0 line measured at an excitation power of $300 \mu\text{W}$. Blue curve is a fitted result including the system function of our setup. From this we deduces $g^{(2)}(0)=0.29$. (Inset) Typical photon count rate variation over 30 min. The count rate fluctuation (1σ) is less than 3%.

respectively. From these results, we obtain a high photon collection efficiency of $\eta_{\text{collect}}=0.435$. That is, 43.5% of photons emitted to air from the QD were collected by the 1st lens of the FCM. The collection efficiency of unidirectional photon flux from a point source by a lens with a given NA value is given by $1-\cos(\sin^{-1} \text{NA})$, which is 0.40 for $\text{NA}=0.8$. This very close agreement demonstrates that the single QD we studied is very precisely aligned to the focal length of the FCM at the emitted photon wavelength with our proposed method for laser reflection measurements through the FCM.

Once the focus position is adjusted by the piezo positioner, our module exhibits excellent stability. Typical variation in the photon count rate measured by an SSPD over 30 min is shown in the inset of Fig. 4, which reveals the fluctuation less than 3%. Furthermore, the decrease in the count rate was less than 10% after 20h of measurements, and was also robust against the heat cycle between liquid helium and RT (not shown). The overall photon coupling efficiency to an SMF is given by the product of $\eta_{\text{collect}} \cdot \eta_{\text{FCE}}$. Although the η_{FCE} value measured on the FCM was 0.267, we later found that it includes an extrinsic optical loss at the SMF counter connector facet due to laser burnout of contaminants. We re-measured η_{FCE} after exchanging the counter connector to a new one without contamination, and obtained the value of $\eta_{\text{FCE}}=0.394$. Therefore an overall photon coupling efficiency of $\eta_{\text{collect}} \cdot \eta_{\text{FCE}} = 17\%$ is possible with the present method. In the present FCM, the NA values of the second lens and the SMF were different (0.5 and 0.2, respectively). If the NA values of the second lens and the SMF are matched, a higher fiber coupling efficiency is expected. Along with the long-term stability of the FCM housing, this demonstrates the possibility of realizing highly stable and efficient fiber-coupled single photon source by extending the present method, e.g., elaborating the photon source structure for directional and gaussian-mode emission.

Acknowledgement

This study was supported in part by the Strategic Information and Communications R&D Promotion Programme (SCOPE) from the Ministry of Internal Affairs and Communications and JSPS KAKENHI Grant Number 15K17456.

References

- 1) L. Atzori, A. Iera, and G. Morabito, *Computer Networks* **54**, 2787 - 2805 (2010).
- 2) N. Gisin, G. Ribordy, W. Tittel, and H. Zbinden, *Rev. Mod. Phys.* **74**, 145–195 (2002).
- 3) S. Buckley, K. Rivoire and J. Vučković, *Rep. Prog. Phys.* **75**, 126503 (2012), and references therein.
- 4) N. Sangouard and H. Zbinden, *J. Mod. Opt.* **59**, 1458–1464 (2012).
- 5) M. B. Ward, O. Z. Karimov, D. C. Unitt, and Z. L. Yuan, P. See, D. G. Gevaux, A. J. Shields, P. Atkinson, and D. A. Ritchie, *Appl. Phys. Lett.* **86**, 201111 (2005).
- 6) T. Miyazawa, K. Takemoto, Y. Sakuma, S. Hirose, T. Usuki, N. Yokoyama, M. Takatsu, and Y. Arakawa, *Jpn. J. Appl. Phys.* **44**, L620–622 (2005).
- 7) I. Suemune, H. Nakajima, X. Liu, S. Odashima, T. Asano, H. Iijima, J. -H. Huh, Y. Idutsu, H. Sasakura, and H. Kumano, *Nanotechnology* **24**, 455205 (2013).
- 8) K. G. Lee, X. W. Chen, H. Eghlidi, P. Kukura, R. Lettow, A. Renn, V. Sandoghdar, and S. Götzinger, *Nat Photon* **5**, 166–169 (2011).
- 9) Y. Ma, P. E. Kremer, and B. D. Gerardot, P. Kukura, R. Lettow, A. Renn, V. Sandoghdar, and S. Götzinger, *J. Appl. Phys.* **115**, 023106 (2014).
- 10) X. -W. Chen, S. Götzinger, and V. Sandoghdar, *Opt. Lett.* **18**, 3545–3547 (2011).
- 11) J. Claudon, J. Bleuse, N. S. Malik, M. Bazin, P. Jaffrennou, N. Gregersen, C. Sauvan, P. Lalanne, and J. -M. Gérard, *Nat Photon* **4**, 174–177 (2010).
- 12) M. E. Reimer, G. Bulgarini, N. Akopian, M. Hocevar, M. B. Bavinck, M. A. Verheijen, E. P. A. M. Bakkers, L. P. Kouwenhoven, and V. Zwiller, *Nat Commun* **3**, 737 (2012).
- 13) M. Munsch, N. S. Malik, E. Dupuy, A. Delga, J. Bleuse, J. -M. Gérard, J. Claudon, N. Gregersen, and J. Mørk, *Phys. Rev. Lett.* **110**, 177402 (2013).
- 14) G. Bulgarini, M. E. Reimer, M. Bouwes Bavinck, K. D. Jöns, D. Dalacu, P. J. Poole, E. P. A. M. Bakkers, and V. Zwiller, *Nano Letters* **14**, 4102–4106 (2014).
- 15) K. Takemoto, M. Takatsu, S. Hirose, N. Yokoyama, Y. Sakuma, T. Usuki, T. Miyazawa, and Y. Arakawa, *J. Appl. Phys.* **101**, 081720 (2007).
- 16) K. Takemoto, Y. Nambu, T. Miyazawa, Y. Sakuma, T. Yamamoto, S. Yorozu, and Y. Arakawa, *Sci. Rep.* **5**, 14383 (2015).
- 17) T. Heindel, C. Schneider, M. Lerner, S. H. Kwon, T. Braun, S. Reitzenstein, S. Höfling, M. Kamp and A. Forchel, *Appl. Phys. Lett.* **96**, 011107 (2010).
- 18) O. Gazzano, S. Michaelis de Vasconcellos, C. Arnold, A. Nowak, E. Galopin, I. Sagnes, L. Lanco, A. Lemaître, and P. Senellart, *Nat Commun* **4**, 1425 (2013).

- 19) H. Kumano, H. Nakajima, H. Iijima, S. Odashima, Y. Matsuo, K. Ijiro, and I. Suemune, *Appl. Phys. Express* **6**, 062801 (2013).
- 20) X. Liu, T. Asano, S. Odashima, H. Nakajima, H. Kumano, and I. Suemune, *Appl. Phys. Lett.* **102**, 131114 (2013).
- 21) M. Davanço, M. T. Rakher, W. Wegscheider, D. Schuh, A. Badolato, and K. Srinivasan, *Appl. Phys. Lett.* **99**, 121101 (2011).
- 22) M. Fujiwara, K. Toubaru, T. Noda, H. -Q. Zhao, and S. Takeuchi, *Nano Letters* **11**, 4362–4365 (2011).
- 23) R. Yalla, F. Le Kien, M. Morinaga, and K. Hakuta, *Phys. Rev. Lett.* **109**, 063602 (2012).
- 24) H. Sasakura, X. Liu, S. Odashima, H. Kumano, S. Muto, and I. Suemune, *Appl. Phys. Express* **6**, 065203 (2013).
- 25) G. Shambat, J. Provine, K. Rivoire, T. Sarmiento, J. Harris, and J. Vučković, *Appl. Phys. Lett.* **99**, 191102 (2011).
- 26) S. Chonan, S. Kato, and T. Aoki, *Sci. Rep.* **4**, 4785 (2014).
- 27) N. Ha, X. Liu, T. Mano, T. Kuroda, K. Mitsuishi, A. Castellano, S. Sanguinetti, T. Noda, Y. Sakuma, and K. Sakoda, *Appl. Phys. Lett.* **104**, 143106 (2014).
- 28) X. Liu, N. Ha, H. Nakajima, T. Mano, T. Kuroda, B. Urbaszek, H. Kumano, I. Suemune, Y. Sakuma, and K. Sakoda, *Phys. Rev. B* **90**, 081301 (2014).
- 29) N. Koguchi, S. Takahashi, and T. Chikyow, *J. Cryst. Growth* **111**, 688–692 (1991).
- 30) S. Kimura, H. Kumano, M. Endo, I. Suemune, T. Yokoi, H. Sasakura, S. Adachi, S. Muto, H. Z. Song, S. Hirose, and T. Usuki, *Jpn. J. Appl. Phys.* **44**, L793 (2005).
- 31) H. Nakajima, H. Kumano, H. Iijima, and I. Suemune, *Appl. Phys. Lett.* **101**, 161107 (2012).
- 32) M. Pelton, C. Santori, J. Vučković, B. Zhang, G. S. Solomon, J. Plant, and Y. Yamamoto, *Phys. Rev. Lett.* **89**, 233602 (2002).